

# Synthesis, characterization of FAU/EMT intergrowths and its catalytic performance in *n*-pentane hydroisomerization reaction

L.N. Belandría<sup>a</sup>, C.S. González<sup>b</sup>, F. Aguirre<sup>a</sup>, E. Sosa<sup>a</sup>, A. Uzcátegui<sup>a</sup>,  
G. González<sup>b</sup>, J. Brito<sup>c</sup>, S.L. González-Cortés<sup>a</sup>, F.E. Imbert<sup>a,\*</sup>

<sup>a</sup> Laboratorio de Cinética y Catálisis, Facultad de Ciencias, Universidad de Los Andes (ULA), La Hechicera, Mérida, Venezuela

<sup>b</sup> Laboratorio de Ciencias e Ingeniería de Materiales, Dpto. Ingeniería, Instituto Venezolano de Investigaciones Científicas (IVIC), Carretera Panamericana Km 11, Altos de Pipe, Los Teques, Venezuela

<sup>c</sup> Laboratorio de catálisis y fisicoquímica de superficies, Centro de Química, Instituto Venezolano de Investigaciones Científicas (IVIC), Carretera Panamericana Km 11, Altos de Pipe, Los Teques, Venezuela

Available online 14 September 2007

## Abstract

Zeolites FAU, EMT and their intergrowths were synthesized using 15-crown-5, 18-crown-6 and their equimolar mixture, respectively. The synthesized products were characterized by XRD, SEM-EDX, N<sub>2</sub> adsorption and TPD-NH<sub>3</sub>. The solids obtained were all highly crystalline. The FAU samples were formed by octahedral submicrometric crystallites, EMT samples had hexagonal plate morphology of 2–5 μm. The intergrowth crystals were micrometric hexagonal plates through whose hexagonal faces, the octahedral FAU crystallites intergrow. The intergrowth proportion was evaluated by means of DIFFaX, resulting in different intergrowth proportions, depending on the molar ratio of template/Al<sub>2</sub>O<sub>3</sub> and on the relative template proportion used in the synthesis gel. For a template/Al<sub>2</sub>O<sub>3</sub> ratio of 0.70, a 50%FAU/50%EMT intergrowth proportion was obtained, with cluster-type stacking and for template/Al<sub>2</sub>O<sub>3</sub> of 0.30 the intergrowth proportion was 12%FAU/88%EMT with two stacking arrangements: clusters and random. Platinum was incorporated to these zeolites and their intergrowths by solid ion exchange; the metal dispersion was evaluated by TEM. For most catalysts the platinum particles were between 4 and 10 nm. All the catalysts were active for *n*-pentane conversion. The activity was found to be a function of acidity. The intergrowth catalysts were the most active materials. The *iso*-pentane selectivity, at 350 °C and carrier gas composition of H<sub>2</sub>:N<sub>2</sub> = 2:1, was 82% independent of time on stream, acidity, Pt/Al ratio and Pt dispersion. The selectivity increased with decreasing temperature and as carrier gas composition became richer in H<sub>2</sub>. The catalytic remaining activity (at 10 min) decreased in the following order: FAU > EMT > intergrowth.

© 2007 Elsevier B.V. All rights reserved.

**Keywords:** Intergrowth; FAU-EMT; Hydroisomerization; *n*-Pentane; Platinum

## 1. Introduction

The zeolite FAU is one of the most important zeolites for catalytic applications, due to its pore size and acid site accessibility. This zeolite has a cubic unit cell, a supercage (~1.2 nm<sup>3</sup>) with four 12-member ring pore openings (0.74 nm), its space group is *Fd3m*, and can be described by the stacking of sodalite layers in a ABCABC sequence [1]. These layers are related by center of inversion in the double six-member rings. The EMT zeolite was synthesized for the first time in 1990 [2]. This has a hexagonal

structure with a space group *P63/mmc*, the stacking of layers results in a ABAB sequence, with a reflection relation between neighbouring layers. Its arrangement of sodalite cages creates “hypocage” [3] (0.5 nm<sup>3</sup>) with three 12-member ring pore openings and a larger cage – ‘hypercage’ [4] (1.3 nm<sup>3</sup>) – with five 12-member ring pore openings. The channel system is tridimensional as in FAU structure, but the nature of the channel system and of the larger cages in the EMT is significantly different. Both structures (i.e. FAU and EMT) have tridimensional systems of large pores and cages. These structures can relate one to another, by changing one element of symmetry by the other between neighbouring sheets. Solids with different stackings of cubic and hexagonal sheets like ZSM-3 [5], ZSM-20 [6–8] and CSZ-1 [9,10] have been reported. The distribution of the two symmetry elements between the layers may be influenced by

\* Corresponding author. Tel.: +58 274 2401371; fax: +58 274 2401360.

E-mail addresses: [gemagonz@ivic.ve](mailto:gemagonz@ivic.ve) (G. González), [joabrito@ivic.ve](mailto:joabrito@ivic.ve) (J. Brito), [imbert@ula.ve](mailto:imbert@ula.ve) (F.E. Imbert).

the template molecules and their proportion in the synthesis gel. The geometry of the cage system is strongly dependent on the actual stacking sequence. In this case the stacking faults do not block the channels, but the local environments are slightly different, so some of the properties of the intergrowth can differ from those of the pure end members. For industrial applications the preparation of metal catalysts should be as simple and economical as possible. Among the methods to introduce metals into zeolites, impregnation and ion exchange are the most used. Ion exchange results in high initial dispersion, while impregnation, that involves mixing the zeolite with a solution of metal precursor followed by evaporation, drying and calcination steps, leads to rather weak metal support interaction [11]; thus, large particles are usually obtained. The conventional liquid ion exchange is limited by precursors solubility, steric hindrance, due to bulky hydration shell of the exchangeable cations and thermodynamic equilibrium [12,13]. To overcome this drawback, some times it is necessary to repeat the exchange procedure several times and to undertake intermediate calcination in order to facilitate cation migration [13,14]. Another disadvantage for industrial applications is the handling of large volume of solution, during the preparation process. The solid-state ion exchange is a highly effective method to introduce cations into zeolite. In this process, the metal cations are introduced into the zeolite by calcination (usually in vacuum or under inert gas flow) of mechanical mixture of the zeolite (usually in protonic form) and the metal precursor (usually halide or oxide) [14]. The major advantage of this method is to incorporate the metal in one step with high dispersion. Hence, in the present work, the solid-state ion exchange, followed by H<sub>2</sub> reduction was used to prepare bifunctional catalysts. The FAU/EMT intergrowth synthesis has been reported in the literature [15–18]. However, we have found a very few reports on FAU/EMT intergrowth catalytic activity [19–22]. The objective of the present work is to study the catalytic behavior of FAU/EMT intergrowth and to compare with pure FAU and EMT, on the *n*-pentane hydroisomerization reaction, which has particular interest for hydrocarbon refining industry.

## 2. Experimental

### 2.1. Catalyst preparation and characterization

The zeolites FAU and EMT were synthesized using as templates (T) 15-crown-5 (1,4,7,10,13-pentaoxacyclopentadecane) (T<sub>1</sub>) and 18-crown-6 (1,4,7,10,13,16-hexaoxacyclooctadecane) (T<sub>2</sub>), respectively [15–18]. The intergrowths were obtained by adding equimolar amounts of these templates to the synthesis gel. The molar composition of the gel used was 10 SiO<sub>2</sub>:Al<sub>2</sub>O<sub>3</sub>:2.1 Na<sub>2</sub>O:T<sub>1</sub> 15-Crown-5:T<sub>2</sub> 18-Crown-6:140 H<sub>2</sub>O, where the template/alumina (T/Al<sub>2</sub>O<sub>3</sub>) molar ratio employed were 0.70 or 0.33.

A sodium aluminate is added to sodium hydroxide under continuous agitation until complete dissolution was attained, then the amount required of the specific template is added, under agitation for 20 min, followed by the addition of colloidal silica. This solution is aged under continuous agitation for 24 h at room temperature, using a special reactor with deflector blades

attached to the walls, to increase homogenization of the gel. Following the ageing period, the reactor is heated at 110 °C for 15 days. The resultant solid was filtered, washed and dried at 80 °C for 16 h. In order to eliminate the template, the samples were calcined at 600 °C for 16 h.

The catalysts were prepared from FAU, EMT and their intergrowth by ion exchange with 2 M NH<sub>4</sub>NO<sub>3</sub> solution, at 80 °C for 24 h, filtered, washed, dried at 120 °C for 4 h and calcined at 450 °C for 4 h, in air; this procedure was repeated several times. However, for EMT (0.33) and 50T<sub>1</sub>/50T<sub>2</sub> (0.33) samples with two different levels of exchange were prepared. One with 100% exchange (no alkaline ions left on the sample), and another was partially exchanged into acid form, that is, part of its exchange positions are still occupied by alkaline ions, decreasing significantly its acidity. In Table 1 a summary of the prepared samples is given with the appropriate synthesis conditions. Once the zeolite acid form was obtained, platinum (~1 wt.%) was incorporated by solid-state ion exchange with Pt(NH<sub>3</sub>)<sub>4</sub>Cl<sub>2</sub>·H<sub>2</sub>O at 500 °C for 4 h, under nitrogen flow. This method has several advantages: avoids handling and disposal of large amounts of solution, cuts down the cost of wasted chemicals as well as the associated environmental impact.

The X-ray diffractograms were recorded in a diffractometer PHILLIPS PW 1050/25 using a Cu Kα (λ = 1.5406 Å) radiation, in the 2θ interval from 5° to 70° and a path of 0.02°. The surface areas and pore volume were measured in a Micromeritics analyser, model ASAP 2010 at liquid nitrogen temperature (77 K). The EDX chemical semiquantitative analysis was made in an EDAX system, model 8400. The scanning was done on a Hitachi Field emission FE, model S-4500 and el transmission electron microscopy analysis on a Philips, model CM10. The acidity was evaluated by NH<sub>3</sub>-programmed thermodesorption and metal dispersion by the CO chemisorption measurements, both were carried out on a Micromeritics TPD/TPR 2900.

### 2.2. Catalytic test

The hydroisomerization reaction was investigated in the temperature range of 250–350 °C, the effect of the carrier gas composition was investigated for the H<sub>2</sub>:N<sub>2</sub> = 30:0, 20:10, 10:20 at atmospheric pressure. A 30 mL/min flow of H<sub>2</sub>:N<sub>2</sub> mixture saturated with *n*-pentane at –3 °C, was fed to a pyrex down flow continuous fixed bed reactor, in line with a gas chromatograph (Perkin-Elmer, Auto System), equipped with an alumina/KCl

Table 1  
Samples prepared

Sample	T/Al <sub>2</sub> O <sub>3</sub>	pH	exchange
HFAU (without template)	0	9	Fully
HFAU (pH = 9)	0.7	9	Fully
HFAU (pH = 11)	0.7	11	Fully
EMT (0.33)	0.33	9	Partially
HEMT (0.33)	0.33	9	Fully
HEMT (0.7)	0.7	9	Fully
FAU/EMT (0.33)	0.33	9	Partially
HFAU/HEMT (0.33)	0.33	9	Fully
HFAU/HEMT (0.7)	0.7	9	Fully

PLOT capillary column, a FID and an integrator PE Nelson model 1022. Before each reaction, the catalyst was reduced *in situ*, in a hydrogen flow of 30 mL/min at 450 °C for 4 h [20–22].

### 3. Results and discussion

#### 3.1. Catalyst characterization

The zeolites FAU, EMT and their intergrowth highly crystalline were obtained, as shown by the powder X-ray diffraction, scanning electron microscopy and specific surface areas. These solids show nitrogen adsorption isotherms type I (Langmuir) typical of micropore solids (see Fig. 1). In Table 2 are given the specific surface area values for as-synthesized samples. As can be seen in Table 2, these zeolites have high Langmuir surface areas. The external surface areas are, as expected, very small.

Table 2

Langmuir ( $A_{Lang}$ ,  $m^2/g$ ), micropore ( $A_m$ ,  $m^2/g$ ) and external ( $A_{ext}$ ,  $m^2/g$ ) specific surface areas, and micropore volume ( $V_m$ ,  $cm^3/g$ )

Catalysts	t-plot			
	$A_{Lang}$ ( $m^2/g$ )	$A_m$ ( $m^2/g$ )	$A_{ext}$ ( $m^2/g$ )	$V_m$ ( $cm^3/g$ )
FAU (without template)	998	986	12.4	0.34
FAU (pH=9)	1061	1060	1.8	0.38
EMT (0.33)	998	985	12.8	0.34
EMT (0.7)	1073	1067	5.5	0.31
FAU/EMT (0.33)	1044	1035	8.8	0.36
FAU/EMT (0.7)	1067	1060	6.3	0.37

The intergrowth does not affect the total pore volume or the surface area.

Well-defined crystals for FAU and EMT were observed by scanning electron microscopy (SEM) (see Fig. 2). The FAU crys-

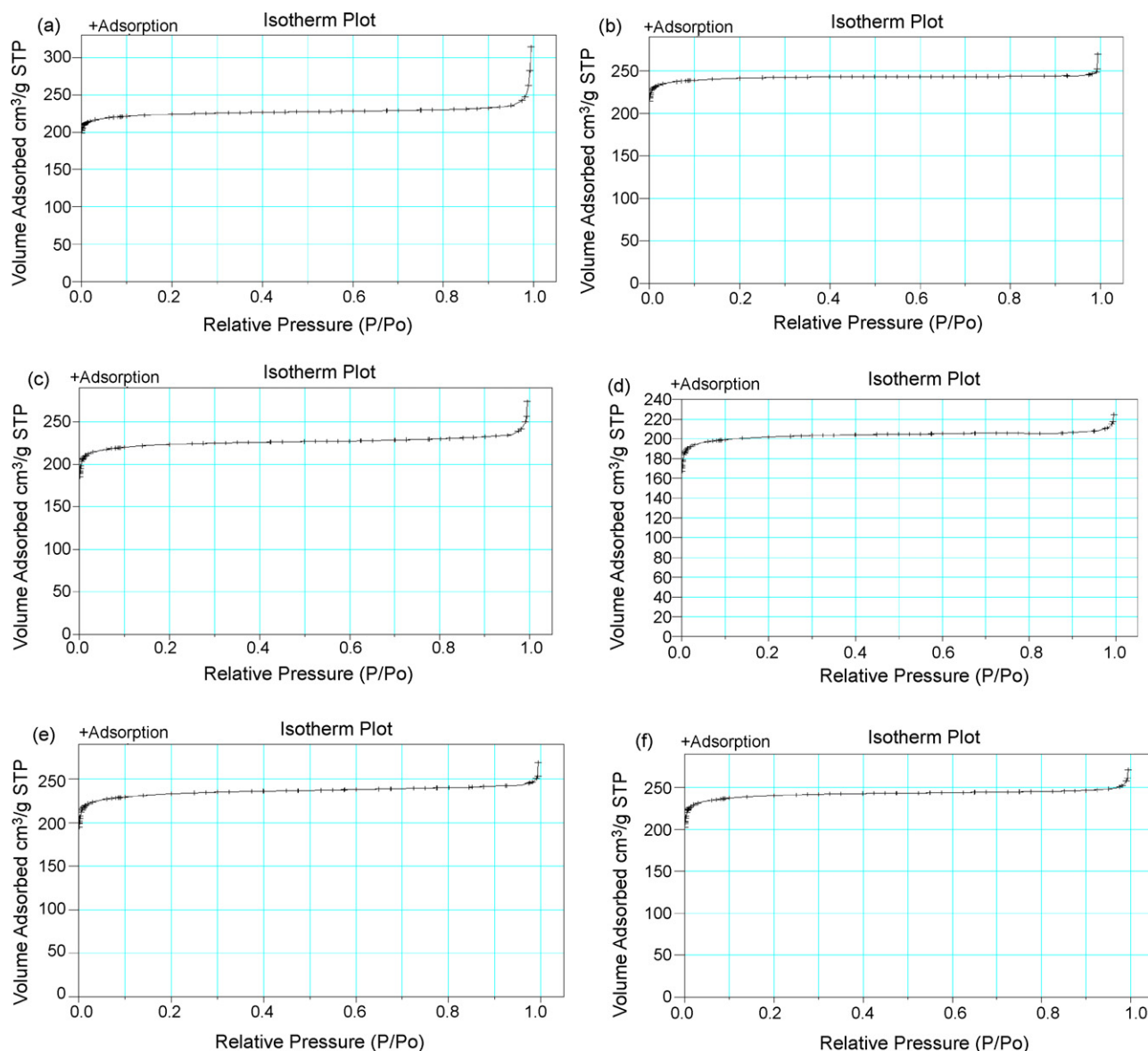


Fig. 1. Adsorption isotherms of  $N_2$  at 77 K, for (a) FAU (without template), (b) FAU (pH=9), (c) EMT (0.33), (d) EMT (0.7), (e) FAU/EMT (0.33) and (f) FAU/EMT (0.7).

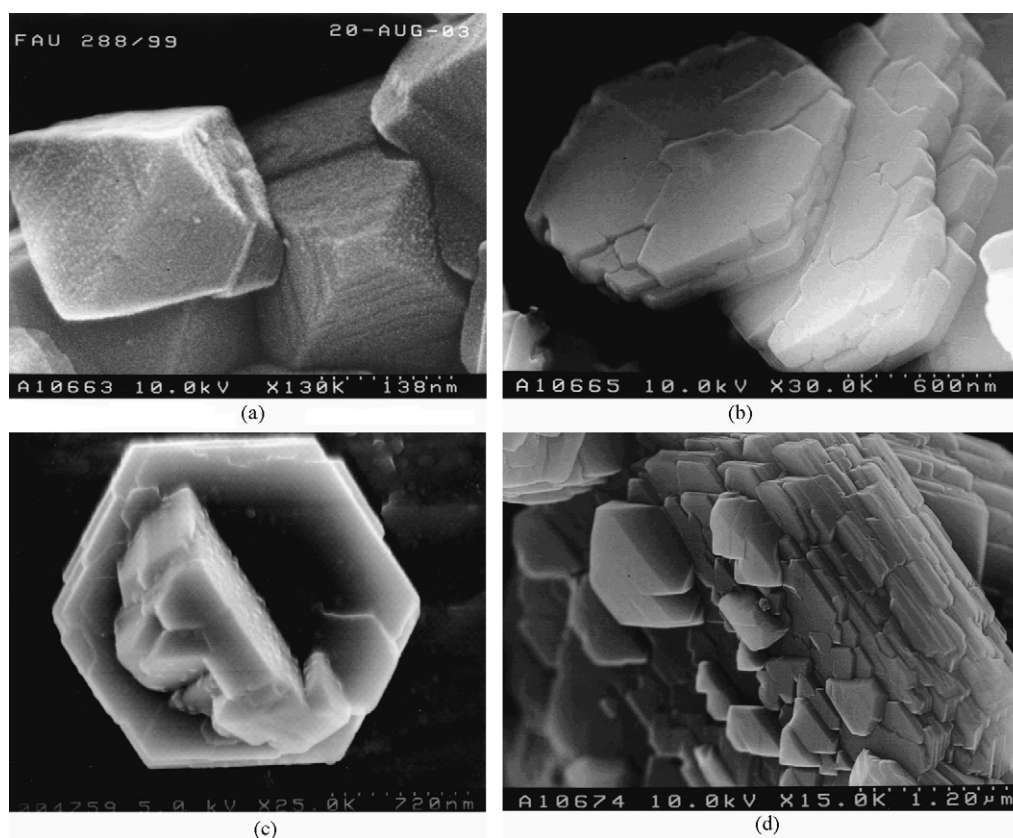


Fig. 2. SEM micrographs of (a) FAU, (b) EMT (0.33), (c) FAU/EMT (0.7) and (d) FAU/EMT (0.33).

tals are octahedral ( $<1 \mu\text{m}$ ), while EMT crystals are hexagonal plates ( $2\text{--}5 \mu\text{m}$ ). The intergrowth crystals are shown in Fig. 2c and d, where one can clearly see the FAU octahedral crystals growing out from the hexagonal EMT plates. This is strong evidence that supports the result obtained from the DIFFaX analysis for the intergrowth FAU/EMT ‘clusters’ distribution.

Fig. 3a shows the simulated X-ray diffraction patterns of the pure systems overlapped one over the other to show the positions when both phases are present. The X-ray powder pattern does not completely differentiate between the contributions from a mixture of phases or from an intergrowth; in general the presence of defects affects the width and shape of the peaks profile. In order to estimate the proportion and type of intergrowth the DIFFaX programme [23] was used. This software generates the X-ray powder diffraction patterns considering coherent planar defects such as twins and stacking faults. DIFFaX computes the average interference wave function scattered for each layer

from a faulted crystal with a random stacking sequence of layers. In real crystals not only stacking defects are present but also dislocation, crystal size, domains, substitutional atoms, vacancies, etc. also contribute to the diffraction pattern. Although, the matching between the experimental X-ray powder pattern and the simulated one are not completely accurate, a fair approximation is obtained. Fig. 3b and c shows the experimental X-ray diffraction patterns of FAU/EMT intergrowth systems synthesized with  $T/\text{Al}_2\text{O}_3$  of 0.33 and 0.7, respectively. It can be observed that the peaks present coincide with the corresponding positions of FAU and EMT. The intergrowth proportion was evaluated by matching the experimental X-ray diffraction pattern with the simulated pattern generated by DIFFaX [23]. Fig. 4 shows the experimental X-ray pattern corresponding to FAU/EMT synthesized with  $T/\text{Al}_2\text{O}_3 = 0.70$  and the simulated pattern obtained by DIFFaX, assuming a block type random distribution of 50%FAU–50%EMT. As can be seen there is a good

Table 3  
Catalyst chemical composition (% atomic) by EDX

Catalysts	O (%)	Al (%)	Si (%)	Si/Al	Pt (%)	Na (%)	K (%)
Pt/HFAU (without template)	57.8	11.1	31.0	2.8	0.13	–	–
Pt/HFAU (pH=9)	50.8	8.11	38.2	4.7	0.11	–	–
Pt/HFAU (pH=11)	57.7	8.32	33.8	4.1	0.25	–	–
Pt/EMT(0.33)	52.2	9.73	35.3	3.6	0.21	2.56	–
Pt/HEMT(0.7)	56.6	7.72	35.5	4.6	0.19	–	–
Pt/FAU/EMT (0.33)	53.7	9.33	33.6	3.6	0.21	2.90	0.63
Pt/HFAU/HEMT (0.7)	58.4	6.95	34.4	4.9	0.18	–	–

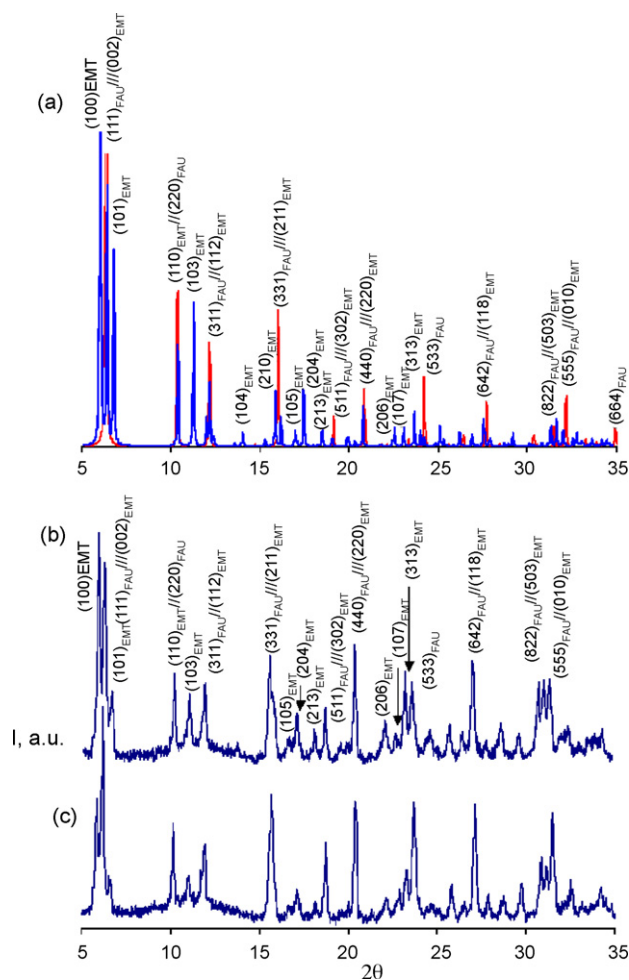


Fig. 3. (a) Simulated XRD diffraction patterns of FAU and EMT pure systems. (b and c) Experimental XRD patterns of intergrowth FAU/EMT for  $(T_1 + T_2)/Al_2O_3$  ratios 0.33 and 0.70, respectively.

agreement between both experimental and simulated patterns. The inset shows an enlarged section of the  $2\theta = 5\text{--}7^\circ$  in order to visualize clearly the similarities between both patterns.

Fig. 5 shows the experimental and simulated patterns for FAU/EMT synthesized with  $T/Al_2O_3 = 0.33$ . Two models of intergrowth distribution were assumed, random stacking of layers and cluster formation. The best fit was obtained for random-stacking layers with a proportion 10%FAU/90%EMT (Fig. 5b). A reasonable match was also obtained for a cluster arrangement with a proportion of 12%FAU/88%EMT (Fig. 5c).

The diffractograms for the catalysts in their final reduced state are shown in Fig. 6. Whatever the catalyst the crystallinity is preserved, except for the FAU sample synthesized without template (Fig. 6a). This sample lost most of its zeolite structure; probably due to its low thermal stability, as a consequence of its low Si/Al ratio. The incorporation of platinum, via solid ion exchange onto all the prepared samples, was confirmed by the peaks at  $2\theta = 39.9^\circ$ ,  $46.4^\circ$  and  $67.6^\circ$ , corresponding to metallic platinum.

The chemical composition is given in Table 3. As can be seen, all the samples were fully decationized, except the sam-

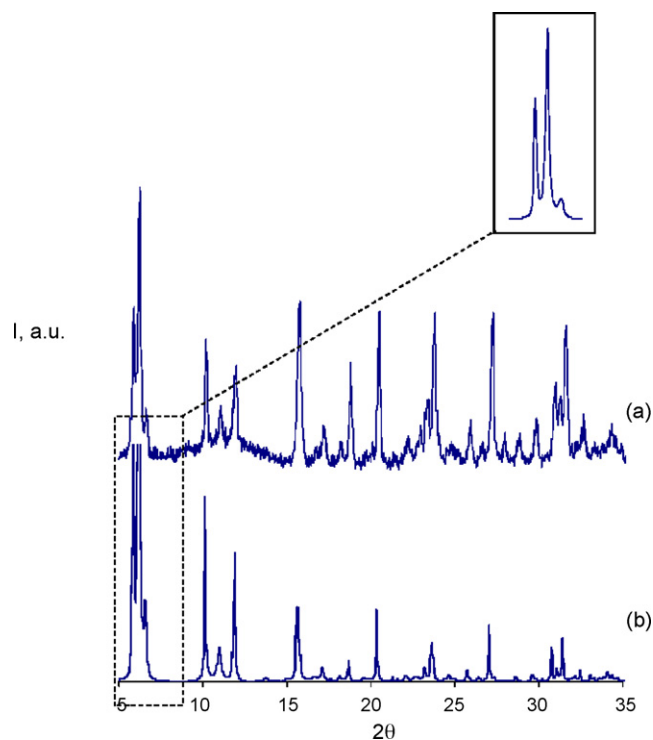


Fig. 4. (a) Experimental XRD pattern of intergrowth FAU/EMT,  $(T_1 + T_2)/Al_2O_3 = 0.70$ . (b) Simulated XRD pattern of intergrowth with stacking of clusters:  $\alpha_{FF} = 0.90$ ;  $\alpha_{EE} = 0.90$ .

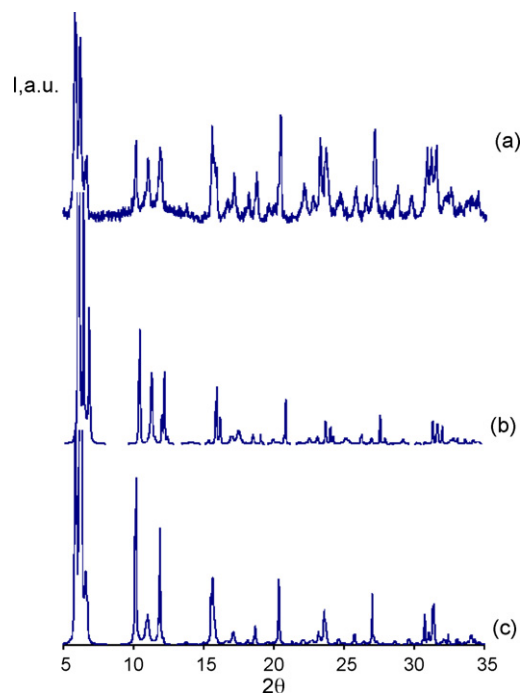


Fig. 5. (a) Experimental XRD pattern for intergrowth with  $(T_1 + T_2)/Al_2O_3 = 0.33$ , (b) simulated for layers with random stackings 10%FAU/90%EMT, and (c) simulated for stacking of clusters of  $\alpha_{FF} = 0.3$  and  $\alpha_{EE} = 0.9$ .

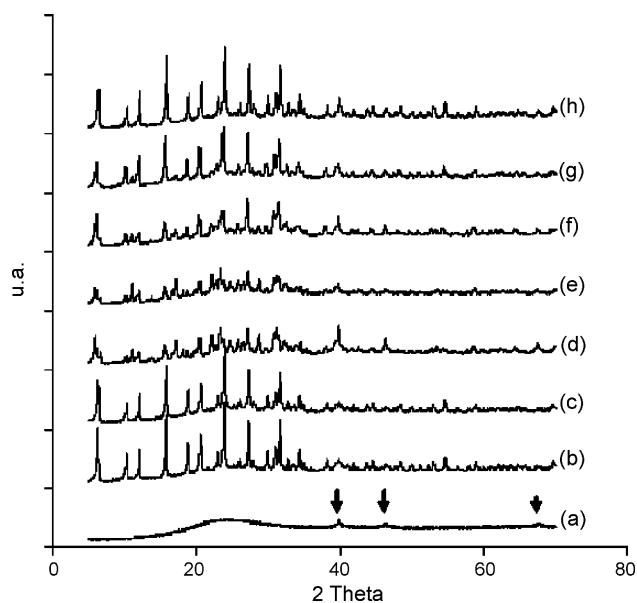


Fig. 6. XRD patterns of Pt-modified zeolite: (a) Pt/HFAU (without template), (b) Pt/HFAU (pH=9), (c) Pt/HFAU (pH=11), (d) Pt/EMT (0.33), (e) Pt/HEMT (0.7), (f) Pt/FAU/EMT (0.33), (g) Pt/HFAU/HEMT (0.7), and (h) Pt/HFAU/HEMT (75/25, 0.7).

ples Pt/EMT(0.33) and Pt/FAU/EMT (0.33), which were only partially exchanged (see Table 1). The Pt/H<sup>+</sup> ratio, the unit cell formula for the zeolites FAU and EMT and the acidity (meqNH<sub>3</sub>/g) are given in Table 4. For FAU synthesized without template, a higher Al content was obtained in the final product. For the FAU structure synthesized with template, the pH increase from 9 to 11 resulted in a slight increase in Al content (lower Si/Al ratio), owing to a higher basicity in the synthesis (see Table 4). The platinum incorporated is also higher for the latter. For the EMT and FAU/EMT series, the increase in T/Al<sub>2</sub>O<sub>3</sub> ratio, from 0.33 to 0.7, decreases Al content (higher Si/Al ratio). For these samples, the higher the Al content, the higher the Pt/H<sup>+</sup> ratio (see Table 4).

The high platinum dispersion was observed by TEM. Highly dispersed platinum nanocrystals can be observed in Fig. 7, for Pt/HEMT (0.7) sample. The crystal sizes were in the range of 4–10 nm for most samples, except for Pt/FAU/EMT (0.33), whose crystal sizes were between 1.5 and 3.5 nm, and for Pt/EMT (0.33) with metal clusters of 20–50 nm (see Table 5).

Table 4  
The Pt/H<sup>+</sup> ratio, unit cell formula and acidity (mequiv.NH<sub>3</sub>/g)

Catalysts	Pt/H <sup>+</sup>	Unit cell	mequiv.NH <sub>3</sub> /g
Pt/HFAU (pH=9)	0.014	H <sub>34</sub> Al <sub>34</sub> Si <sub>158</sub> O <sub>384</sub>	2.06
Pt/HFAU (pH=11)	0.030	H <sub>38</sub> Al <sub>38</sub> Si <sub>154</sub> O <sub>384</sub>	2.35
Pt/EMT(0.33)	0.021	Na <sub>5.5</sub> H <sub>15.5</sub> Al <sub>21</sub> Si <sub>75</sub> O <sub>192</sub>	1.57
Pt/HEMT(0.33)	0.030	H <sub>16.7</sub> Al <sub>16.7</sub> Si <sub>79.3</sub> O <sub>192</sub>	2.58
Pt/HEMT(0.7)	0.024	H <sub>17</sub> Al <sub>17</sub> Si <sub>79</sub> O <sub>192</sub>	2.24
Pt/FAU/EMT (0.33)	0.036	–	1.84
Pt/HFAU/HEMT (0.33)	0.011	–	2.87
Pt/HFAU/HEMT (0.7)	0.026	–	2.55

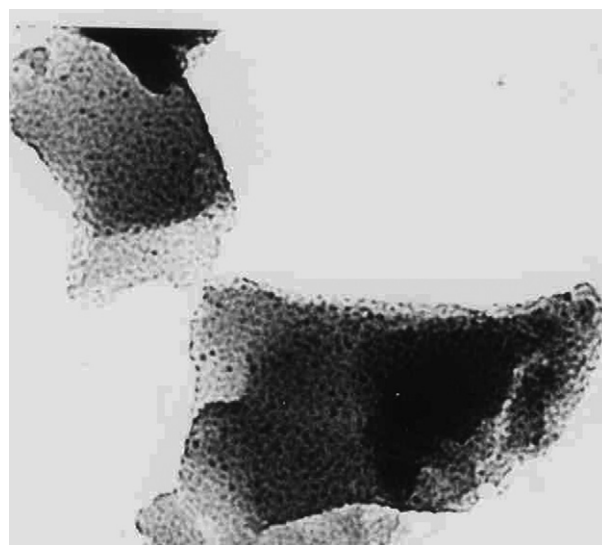


Fig. 7. TEM micrograph of Pt/HEMT (0.70).

### 3.2. Catalytic test

The catalysts were active for *n*-pentane conversion, particularly for hydroisomerization into *i*-pentane. Fig. 8a shows the behavior of Pt/zeolite catalysts prepared from gel composition of T/Al<sub>2</sub>O<sub>3</sub> = 0.7. The Pt/HFAU/HEMT (0.7) intergrowth catalyst showed the highest initial activity for this series. The catalyst prepared from zeolite FAU (pH = 11) was the most active and stable in the series of faujasites, probably due to the slightly higher acidity than that for FAU (pH = 9). Comparing the catalytic performance of the structures synthesized with T/Al<sub>2</sub>O<sub>3</sub> = 0.7, the intergrowth structure shows higher initial catalytic activity than EMT or FAU structures alone, while FAU shows higher residual catalytic activity in the time scale studied (time on stream, *t*<sub>os</sub> = 2–10 min) (see Fig. 8a). The Pt/HEMT sample, showed slightly higher activity than the Pt/HFAU, both synthesized with T/Al<sub>2</sub>O<sub>3</sub> = 0.7 and at pH = 9, but less active than the Pt/HFAU sample, synthesized with T/Al<sub>2</sub>O<sub>3</sub> = 0.7 and at pH = 11. This behavior is in agreement with the catalyst acidity (see Table 4 and Fig. 9), as reported elsewhere [16,24–26].

The catalyst prepared from the zeolite FAU (synthesized without template) was the less active, due to the structural collapse that occurred during catalyst preparation. This low thermal and hydrothermal stability was a consequence of its low Si/Al

Table 5  
Metal dispersion measured by TEM (*d*<sub>Pt</sub>, nm) and by CO chemisorption (*D*, %)

Catalysts	<i>d</i> <sub>Pt</sub> (nm)	<i>D</i> (%)
Pt/HFAU (without template)	4–7	1.1
Pt/HFAU (pH = 9)	4–8	31.1
Pt/HFAU (pH = 11)	4–10	42.0
Pt/EMT (0.33)	20–50 clusters	17.6
Pt/HEMT (0.33)	–	7.53
Pt/HEMT (0.7)	5	57.9
Pt/FAU/EMT (0.33)	1.5–3.5	9.58
Pt/HFAU/HEMT (0.33)	–	10
Pt/HFAU/HEMT (0.7)	6	14.4

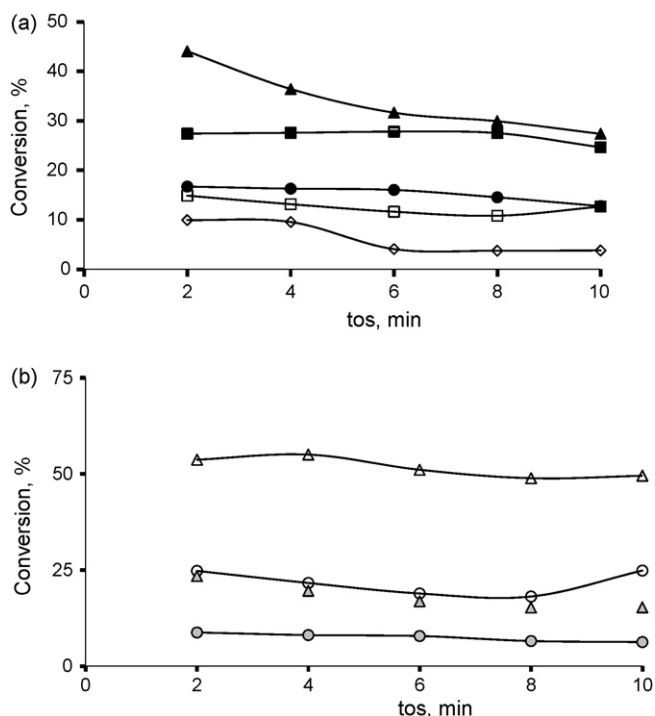


Fig. 8. Conversion (%) as function of the time on the stream (os, min) for (a) zeolites Pt/HFAU: (■) pH=11; (□) pH=9; (◇) without template, (▲) Pt/HFAU/HEMT (0.7) and (●) Pt/HEMT (0.7) and (b) (○) zeolites Pt/HEMT (0.33); (◐) Pt/EMT (0.33); (△) Pt/HFAU/HEMT (0.33); (◔) Pt/FAU/EMT (0.33).

ratio [27]. However, the catalyst shows some activity, probably associated to the presence of platinum active sites.

The behavior of Pt/EMT (0.33) and Pt/FAU/EMT (0.33) catalysts, with different amount of alkaline cation (see Table 3), is shown in Fig. 8b. For both partially and totally decationized samples the intergrowth structures are more active. The higher the degree of proton exchange, the higher the activity for EMT and for the intergrowth structure. Therefore, not only the acid sites in the supercages for FAU and in the hypercages for EMT structures, but also the acid sites in the hypocages for EMT structures do participate in the reaction. The Pt/HFAU/HEMT (0.33) intergrowth catalyst showed the highest activity for this series. In general, it appears that the structures synthesized with a  $T/Al_2O_3 = 0.33$  are more active than those synthesized with a  $T/Al_2O_3 = 0.7$ . This is probably related to the fact that at

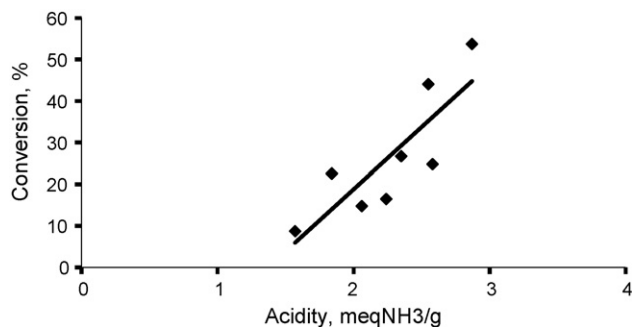


Fig. 9. Conversion (%) as function of acidity (mequiv.NH<sub>3</sub>/g) for all catalysts.

low  $T/Al_2O_3$  ratio the aluminum incorporation into the structure is favoured, with the corresponding increase in acidity (see Table 4).

For this series, one can see that the catalyst activity increases with its acidity, as can be seen in Fig. 9, where the initial conversion (%) (at 2 min) is plotted versus total acidity (mequiv.NH<sub>3</sub>/g). In the range studied, neither the Pt/H<sup>+</sup> ratio nor the metal dispersion had an observable effect on activity. On the contrary, the intergrowth structures do have a pronounced effect on activity. Thus, the FAU/EMT (0.33) has an intergrowth proportion of 10%FAU/90%EMT, whereas FAU/EMT (0.7) has 50%FAU/50%EMT, and this is reflected in the activity. This appears to suggest that the intergrowth enhances the catalyst activity. The lower activities for Pt/EMT (0.33) or Pt/FAU/EMT (0.33) are due to the presence of alkaline cations that limit the acidity (see Tables 3 and 4), stressing the key role played by the acid sites in determining the catalyst activity [28–31].

At 350 °C and with a carrier gas flow composition of H<sub>2</sub>:N<sub>2</sub> = 2:1, the *iso*-pentane yield appeared to be a direct function of conversion, as shown in Fig. 10, for whatever structure (i.e. FAU, EMT or FAU/EMT) and at different times on stream. The slope of this curve is the selectivity; therefore, it appears to be independent of structure, time on stream, acidity, Pt/H<sup>+</sup> ratio and metal dispersion, for this series of catalysts under these conditions (given temperature and carrier gas composition). From the slope is obtained a value of 82% selectivity, which is slightly higher than the one reported in the literature (72%) [32]. This value compares very well with that calculated, using a Gibbs free energy of  $-1.18$  kcal/mol [33]. In fact, for Pt/MOR catalyst, it has been reported that the selectivity is a function both of conversion and of the degree of deactivation [34].

The residual activity at 10 min, measured as the ratio of conversion ( $X_{10}$ , %) at 10 min to initial conversion at 2 min ( $X_2$ , %) is given in Table 6. For such short range of time, the residual catalytic activity is in the order FAU > EMT > intergrowth. Dougnier et al. [16] reported similar results for the cracking of

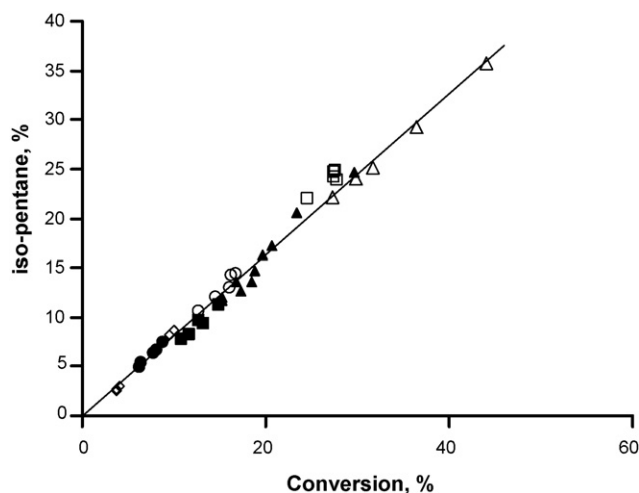


Fig. 10. *iso*-pentane yield (%) as function of conversion (%) for zeolites Pt/HFAU: (□) pH = 11; (■) pH = 9; (◇) without template; (○) zeolites Pt/HEMT (0.7); (●) Pt/EMT (0.33); and intergrowths: (△) Pt/HFAU/HEMT (0.7) and (▲) Pt/FAU/EMT (0.33).

Table 6  
Remaining activity at 10 min ( $X_{10}/X_2$ )

Catalysts	$X_{10}/X_2$
Pt/FAU (without template)	0.38
Pt/HFAU (pH = 9)	0.85
Pt/HFAU (pH = 11)	0.90
Pt/EMT (0.33)	0.72
Pt/HEMT (0.33)	0.73 <sup>a</sup>
Pt/HEMT (0.70)	0.76
Pt/FAU/EMT (0.33)	0.65
Pt/HFAU/HEMT (0.33)	0.92
Pt/HFAU/HEMT (0.7)	0.62

<sup>a</sup> The remaining activity was calculated at 8 min on stream,  $X_8/X_2$ .

*n*-heptane and Berreghis et al. [28] for the hydrocracking of *n*-heptane. However, for Pt/HFAU/HEMT (0.33) residual activity is comparable with that of template-synthesized Pt/HFAU.

The increase in the  $H_2:N_2$  carrier composition, leads to higher activity, stability and selectivity, as shown in Fig. 11, due to the increase in the hydrogenation of olefins. This fact inhibits the coke precursor formation, which is the main cause of catalyst deactivation and enhances the selectivity to isoparaffins through hydrogenation of intermediate branched olefins.

The intergrowth FAU/EMT is a highly active and selective catalyst. For the intergrowth Pt/HFAU/HEMT (0.33), the conversion increases with the reaction temperature, while selectivity to *i*-pentane increases and approaches 100% with decreasing temperature, as shown in Fig. 12. The isomerization at low temperature is enhanced, since this is an exothermic reaction. While at higher temperatures the endothermic reactions such as cracking become more important.

The studied catalyst was highly selective to *i*-pentane. However, some minor products were also observed. Among them,

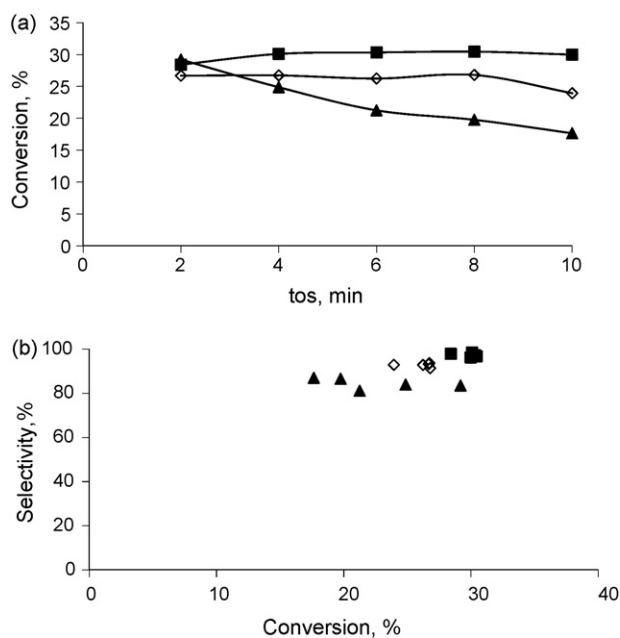


Fig. 11. (a) Conversion (%) as a function of time on stream (min). (b) selectivity (%) as a function of conversion (%), at  $T = 350^\circ\text{C}$ ,  $H_2:N_2 = 30:0$  (■);  $20:10$  (◇);  $10:20$  (▲); for Pt/HFAU (0.7).

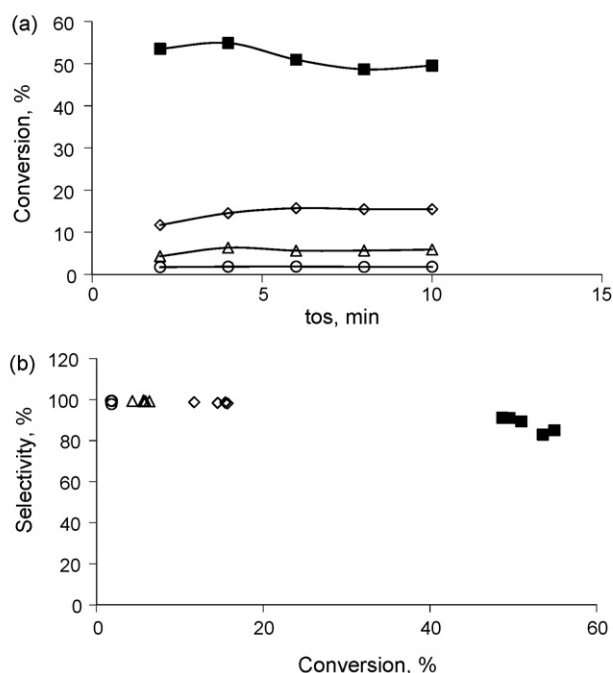


Fig. 12. (a) Conversion (%) as a function of tos (min). (b) selectivity (%) as a function of conversion (%), for  $T = 350^\circ\text{C}$  (■);  $300^\circ\text{C}$  (◇);  $275^\circ\text{C}$  (△);  $250^\circ\text{C}$  (○);  $H_2:N_2 = 2:1$ , on Pt/HFAU/HEMT (0.33).

methane, ethane, propane, *i*-butane and *n*-butane, were reported as cracking products, pentenes reported as dehydrogenation products, and those with carbon numbers higher than five are reported as C5+. In Fig. 13, minor product distribution is presented. The presence of cracking and C5+ fractions can be explained by C5 disproportionation to C4+C6 and to C3+C7. C6 and C7 can undergo cracking to C3 and C4. These products can also be explained by C5 dimerization to C10, followed by a fast isomerization and cracking to C4+C6 and to C3+C7. Comparing the catalysts Pt/HEMT(0.33), Pt/EMT(0.33), Pt/HFAU/HEMT(0.33) and Pt/FAU/EMT (0.33), it can be seen that the cracking activity increases with the degree of protonic exchange. This probably is due to the increase in the amount and strength of accessible acid sites.

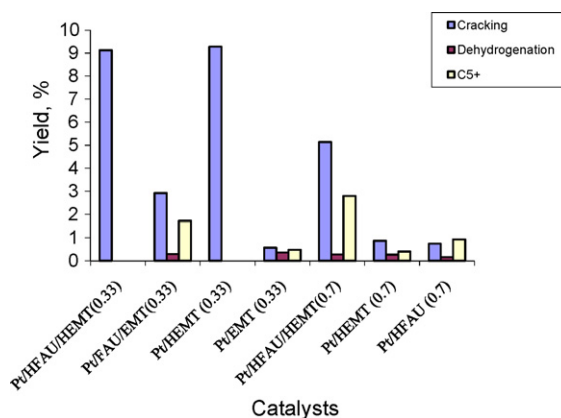


Fig. 13. Cracking (%), dehydrogenation (%) and C5+ (%) yield at  $350^\circ\text{C}$ ,  $H_2/N_2 = 20/10$ .

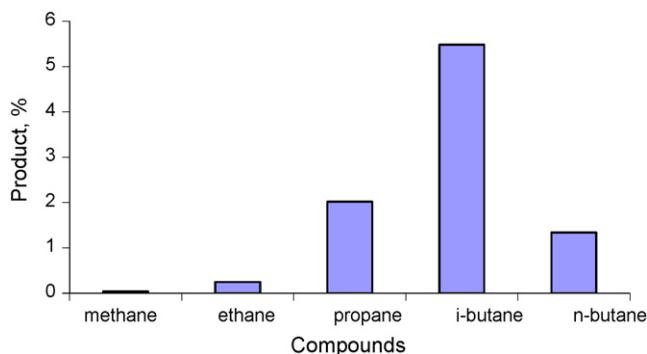


Fig. 14. Typical cracking product distribution.

The Fig. 14 shows the typical cracking product distribution observed for these catalysts. The major component is *i*-butane, while CH<sub>4</sub> and C<sub>2</sub>H<sub>6</sub> are present at trace level, indicating that the hydrogenolysis reaction is practically insignificant.

#### 4. Conclusions

The intergrowths of zeolites FAU/EMT were synthesized using mixtures of 15-crown-5 and 18-crown-6 as templates in the synthesis gels. Well-dispersed platinum was successfully incorporated onto the zeolite via solid-state ion exchange procedure. The catalytic activity of the FAU/EMT intergrowth structure was higher than that for the pure EMT or FAU structures under the same reaction conditions. The structure order of activity was FAU/EMT > EMT ≥ FAU, for samples synthesized at pH = 9 and T/Al<sub>2</sub>O<sub>3</sub> = 0.7. The structure synthesized with lower T/Al<sub>2</sub>O<sub>3</sub> incorporated more aluminum and were more active. The synthesis of FAU structure at pH = 11 lead to a more acidic samples; and consequently, more active. The acidity and the presence of intergrowth structure were the key factors that control the activity. The catalytic remaining activity at 10 min follows the order FAU > EMT > intergrowths FAU/EMT. The selectivity obtained at 350 °C, and a carrier gas flow composition of H<sub>2</sub>:N<sub>2</sub> = 2:1 was 82% independent of structure, time on stream, acidity, Pt/Al ratio or metallic dispersion. The selectivity is, however, a function of temperature and carrier gas composition. Thus, the selectivity increases as the temperature decreases and/or hydrogen content increases in the gas carrier.

#### Acknowledgements

The authors are grateful to the following institutions FONACIT: Agenda Petr leo CONICIT-CONIPET No. 97003795, G-2000001537 and CDCHT-ULA (C-1231-04-08-B), for the financial support.

#### References

[1] H. van Bekkum, E.M. Flanigen, P.A. Jacobs, J.C. Jansen (Eds.), Introduction to Zeolite Science and Practice, 2nd ed., Elsevier, Amsterdam, 2001.  
 [2] F. Delprato, L. Demontte, J.L. Guth, L. Huve, Zeolites 10 (1990) 546.

[3] J.A. Martens, P.A. Jacobs, in: E.G. Derouane, F. Lemos, C. Naccache, F.R. Ribeiro (Eds.), Zeolite Microporous Solids: Synthesis, Structure and Reactivity, NATO ASI Ser. C, Vol. 352, Kluwer, Dordrecht, 1992, p. 511.  
 [4] J.M. Thomas, M. Audier, J. Klinowski, J. Chem. Soc., Chem. Commun. (1981) 1221.  
 [5] G.T. Kokotailo, J. Ciric, Adv. Chem. Ser. 101 (1971) 109.  
 [6] J. Ciric, US Patent 3,972,983 (1976).  
 [7] V. F l p, G. Bob ly, H.K. Beyer, S. Ernst, J. Weitkamp, J. Chem. Soc., Faraday Trans. 85 (1989) 2127.  
 [8] M.M.J. Treacy, J.M. Newsam, D.E.W. Vaughan, K.G. Strohmaier, W.J. Mortier, J. Chem. Soc. Chem. Commun. (1989) 493.  
 [9] D.E.W. Vaughan, M.G. Barret, US Patent 4,309,313 (1982).  
 [10] M.M.J. Treacy, J.M. Newsam, R.A. Beyerlein, M.E. Leonowicz, D.E.W. Vaughan, J. Chem. Soc. Chem. Commun. (1986) 1211.  
 [11] P. Canizares, A. de Lucas, F. Dorado, A. Duran, I. Asencio, Appl. Catal. A: Gen. 169 (1998) 137.  
 [12] G. Kinger, A. Lugstein, R. Swagera, M. Ebel, A. Jentys, H. Vinek, Micropor. Mesopor. Mater. 39 (2000) 307.  
 [13] Ch. Jia, P. Beaunier, P. Massiani, Micropor. Mesopor. Mater. 24 (1998) 69.  
 [14] C. Stolz, A. Sauvage, P. Massiani, R. Kramer, Appl. Catal. A: Gen. 167 (1998) 113.  
 [15] N. Hanif, M.W. Anderson, V. Alfredsson, O. Terasaki, Phys. Chem. Chem. Phys. 2 (2000) 3349.  
 [16] F. Dognier, J. Patarin, J.L. Guth, D. Anglerot, Zeolites 12 (1992) 160.  
 [17] C.S. Gonz lez, S ntesis y caracterizaci n de sistemas de intercrecimiento FAU/EMT, Tesis de Maestr a, Instituto Venezolano de Investigaciones Cient ficas (IVIC), 2004.  
 [18] G. Gonz lez, C.S. Gonz lez, Proceedings of XVII Simposio Iberoamericano de Cat lisis, Margarita (Venezuela), 2002, p. 150.  
 [19] J.A. Martens, P.A. Jacobs, J. Mol. Catal. 78 (1993) L47–L52.  
 [20] L.N. Beldr ria R., Trabajo Especial de Grado, Universidad de Los Andes, M rida-Venezuela, 2004.  
 [21] L.N. Beldr ria, C.S. Gonz lez, J.C. Hern ndez, A. Uzc tegui, G. Gonz lez, J. Brito, A. Calafat, F. Arenas, F. Imbert, Proceedings of 13<sup>o</sup> Congreso Brasileiro de Cat lisis and 3<sup>o</sup> Congreso de Cat lisis del Mercosur, Foz de Iguazu-Brasil, 2005.  
 [22] L.N. Beldr ria, C.S. Gonz lez, J.C. Hern ndez, A. Uzc tegui, G. Gonz lez, J. Brito, A. Calafat, F. Arenas, F. Imbert, Proceedings of XX Simposio Iberoamericano de Catalisis, Gramados, Brazil, 2006.  
 [23] M.M.J. Treacy, J.M. Newsam, M.W. D em, Proc. Roy. Soc. Lond. A 433 (1991) 499.  
 [24] G. Lischke, E. Schreier, B. Parltitz, I. Pitsch, U. Lohse, M. Woettke, Appl. Catal. A: Gen. 129 (1995) 57.  
 [25] Y. Cao, R. Kessas, C. Naccache, Y. Ben Taarit, Appl. Catal. A: Gen. 184 (1999) 231.  
 [26] T. Rorvik, H. Mostad, O. Henrik Ellestad, M. St cker, Appl. Catal. A: Gen. 137 (1996) 235.  
 [27] G. Giannetto, A. Montes, G. Rodr guez, Zeolitas: Caracter sticas, Propiedades y Aplicaciones Industriales, Editorial Innovaci n Tecnol gica, UCV, Caracas, Venezuela, 2000.  
 [28] A. Berreghis, P. Magnoux, M. Guisnet, Proceedings of 12th International Zeolite Conference, vol. IV, Baltimore, USA, July 5–10, 1998, pp. 2719–2726.  
 [29] L.O. Almanza, T. Narbeshuber, P. d’Araujo, C. Nacache, Y.B. Taarit, Appl. Catal. 178 (1999) 39.  
 [30] A. Holl , J. Hancs k, D. Lall , Appl. Catal. 229 (2002) 93.  
 [31] M. Weihe, M. Hunger, M. Breuninger, H.G. Karge, J. Weitkamp, J. Catal. 198 (2001) 256.  
 [32] F. Schmidt, E. Kohler, in: M. Guisnet, P. Gilson (Eds.), Zeolites for Cleaner Technologies, Imperial College Press, London (Great Britain), 2002, p. 153 (chapter 7).  
 [33] D. Stull, E. Westrum, G. Sinke, The Thermodynamics of Organic Compounds, New York (USA), 1969.  
 [34] A. Corma, A. Mart nez, in: M. Guisnet, P. Gilson (Eds.), The Chemistry of the catalytic process, in Zeolites for Cleaner Technologies, Imperial College Press, London (Great Britain), 2002, p. 29 (chapter 2).